PHYSIOGRAPHIC AND CLIMATIC CONTROLS ON THE SPATIAL DISTRIBUTION OF ROCK GLACIERS AND PERIGLACIAL LANDFORMS IN THE DRY ANDES, SAN JUAN, ARGENTINA

by

Adam Trzinski

A thesis submitted to the Faculty of the University of Delaware in partial fulfillment of the requirements for the degree of Master of Science in Geology

Spring 2017

PHYSIOGRAPHIC AND CLIMATIC CONTROLS ON THE SPATIAL DISTRIBUTION OF ROCK GLACIERS AND PERIGLACIAL LANDFORMS IN THE DRY ANDES, SAN JUAN, ARGENTINA

by

Adam Trzinski

Approved: ____
Michael A. O'Neal, Ph.D.
Professor in charge of thesis on behalf of the Advisory Committee

Approved: ____
Neil C. Sturchio, Ph.D.
Chair of the Department of Geological Sciences

Approved: ____
Mohsen Badiey, Ph.D.
Dean of the College of Earth, Ocean, and Environment

Approved: ____
Ann L. Ardis, Ph.D.
Senior Vice Provost for Graduate and Professional Education

ACKNOWLEDGMENTS

I would like to thank all of the people who made this thesis possible. I am grateful for Dr. Michael O'Neal for providing me with multiple trips to South America, as well as for his guidance and patience in working with me the past two years. I would like to thank my committee members, Dr. Brian Hanson and Tracy DeLiberty for their enormous assistance and suggestions throughout the project. I also must thank Dr. Claire O'Neal, for her exceptionally helpful edits and kindness.

Fieldwork in the Andes was made possible by the support of Dr. Andres Meglioli of Mountain Pass LLC. I must thank Coty Cribb, Adrienne Shumlich, and Juampi Dominguez for sharing the high elevation labor and Argentine culture with me. I am also appreciative of Erika Schreiber's above and beyond assistance in understanding her previous work in this area.

Lastly, I would like to thank the people who have supported me through graduate school. This thesis would not have been possible without the friendship that I found in Delaware. To my numerous friends, I am forever grateful for the enjoyment that I experienced during this process. Bennie Dollard's contributions also significantly aided my work. Finally, I thank my parents and the boys, for unconditionally standing by me and rooting for my happiness and success my entire life.

TABLE OF CONTENTS

LIST OF TABLES

LIST OF FIGURES

ABSTRACT

Recent environmental legislation in Argentina seeks to protect and preserve glacier ice, including that in ice-saturated landforms with debris cover like many rock glaciers and protalus ramparts, as important water reserves in the Dry Andes. Although ice exposed at the surface is easy to identify, the extent of buried ice coverage – and therefore its impact on regional hydrology – is not well known in this remote and little-studied terrain. This study investigates the physiographic, geographic, and climatic factors controlling the distribution of rock glaciers and periglacial landforms using a digital inventory spanning a 2400 km^2 area of the Dry Andes in the San Juan Province, Argentina. Multivariate analyses of the inventory data reveal that the presence and size of these landforms are largely controlled by the properties of their adjacent talus supply area. In the talus supply area, colder annual ground temperatures, higher average elevations, larger surface areas, and south-trending aspects highly correlate with larger and less elongated periglacial landforms. These results and the statistics of the inventory indicate the preferred conditions of elevation, slope, aspect, and solar radiation, where rock glaciers and other periglacial landforms, and potentially ground ice, are located. The methods and results provided in this study can be applied to other areas in the Dry Andes to identify analogous conditions, aiding land-use and environmental protection decisions.

Chapter 1

INTRODUCTION

The Argentine National Glacier Act of 2010 was designed to preserve glacial and periglacial environments with the assumption that ice-rich landforms contribute significantly to the freshwater hydrology of the region (Azócar and Brenning, 2010). Because arid regions like the Dry Andes rely heavily on summer meltwater, it is critical to understand where these possible reservoirs have formed (Azocar and Brenning, 2010; Gascoin et al., 2011). As such, the law comprehensively includes protection not just for corporeal, easily identifiable glaciers, but also frozen ground and ice-saturated periglacial landforms.

While environmental protection is of great importance to the local agrarian-based population within and near the Dry Andes, precious metals found in large concentrations present enormous and desirable economic growth opportunities. However, extraction of minerals beneath rock glaciers and periglacial landforms may disturb buried-ice resources. Despite the economic interest in the mineral-resource-rich Dry Andes, little is known about persistent ice in this difficult-to-access terrain.

To protect areas with persistent ice as possible water resources first requires insights into the spatial distribution of ice-rich landforms, ideally by creating a detailed inventory of their extents and coordinates. Previous studies in the Dry Andes have largely focused on rock glaciers. Rock glaciers have been geomorphically characterized as flowing bodies of ice and debris that form in high, arid regions, generally only at the foot of steep talus slopes (Martin and Whalley, 1987; Barsch, 1996; Haeberli et al., 2006; Gruber, 2009; Harris et al., 2009). In the Dry Andes, studies have sought to create rock glacier inventories (Azocar and Brenning, 2010; Bodin et al., 2010; Lenzano et al., 2010; Falaschi et al., 2014; Rangecraft et al., 2014; Janke et al., 2015) or to assess the geographic distribution of rock glaciers (Perucca and Angillieri, 2007; Angillieri, 2009; Perucca and Angillieri, 2011), and thus understand the impact rock glaciers have on regional hydrology. These studies do not include protalus ramparts, present as stagnant ridges of ice and debris formed by talus cover on annual snowbanks (Ballantyne, 1994; Shakesby et al., 1999), a type of periglacial landform also covered by Argentina's environmental protection law. Importantly, both rock glaciers and protalus ramparts originate via the addition of coarse material from an adjacent talus slope. To our knowledge, no studies have statistically evaluated how the talus supply affects the distribution of rock glaciers and periglacial landforms.

Rock glaciers and other ice-rich landforms can be found at similar latitudes and altitudes (Figure 2), which suggests that predictable factors govern feature formation. The nature of how these factors, each with varying degrees of influence on ground ice formation, impact the formation of ice-saturated landforms is not well understood. Clearly, a better understanding of the environmental factors that promote the persistence of ice-saturated landforms is required to assist responsible land development efforts as they seek to identify sensitive landforms while also utilizing regional economic resources.

This study presents an inventory and a statistical analysis of 309rock glaciers and periglacial landforms over a broad geographical area with desirable mineral resources in the high Dry Andes. Specifically, our study area spans from 31°00'S to 31°32'S and 79°09'W to 79°34'W within the San Juan province of Argentina (Figure 1). The key objectives of this study were to: 1) identify rock glaciers and protalus ramparts using spaceborne imagery; 2) manually digitize boundaries for each landform and adjacent talus supply area; 3) subdivide the inventory into tongue-shaped rock glaciers (rock glaciers), lobate shaped rock glaciers (lobate complexes), and protalus ramparts; 4) analyze the Advanced Spaceborne Thermal Emission and Reflection Radiometer Global Digital Elevation Model (ASTER GDEM) data captured over the study area to extract statistics of elevation, slope, and aspect for each landform and adjacent talus supply area; 5) generate a mean annual ground temperature (MAGT) for each cell of the GDEM via analysis of ground-surface temperatures from a related study (Schreiber, 2015); 6) identify statistically significant relationships between these landforms using a Principal Components Analysis (PCA). Our analysis suggests that physiography (i.e., elevation, slope, and aspect) exerts a primary control on the presence/absence of these periglacial landforms. However, the size and shape of ice-rich landforms depend on the physiography and ground temperatures associated with the adjacent talus source areas that provide new materials. Our findings of these controls can be applied to other areas in the Dry Andes and elsewhere to rapidly screen for analogous conditions where these difficult-to-detect features are likely to have formed, aiding responsible land-use and environmental protections decisions in sensitive regions.

Chapter 2

STUDY AREA AND BACKGROUND

The study area is located in a subregion of the Andes Mountains known as the Cordillera Frontal of the Dry Andes between approximately 31°00'S to 31°32'S along the border of Argentina and Chile (mostly within Argentina). The broader Andes range to which the study area belongs is one of the largest mountain ranges in the world in terms of both area and elevation, second only to the Himalayas. With a length of approximately 7000 km, the Andes encompass nearly the entire western edge of South America from approximately 10°N to 53°S (Strecker et al., 2007; Garreaud 2009). The Andes range has formed as a volcanic belt where the Nazca plate began its subduction beneath the South American plate approximately 200 million years ago (Uyeda and Kanamori, 1979; Cristallini and Ramos, 2000). Paleozoic- to Triassic-age lavas, ignimbrites, and pyroclastic rocks of the Choiyoi Group comprise the basement rock in the study area, with Triassic- to Tertiary-age volcanic rocks dominating the surficial geology (Ramos and Vujovich, 1995; Cristallini and Ramos, 2000; Rabassa and Clapperton, 1990; Heredia et al., 2012). Tectonic compression during the Neogene emplaced copper porphyries that are highly prospected in the study area (Maksaev et al., 2009; Maydagan et al., 2016).

The Dry Andes are perpendicular to moisture-bearing winds that originate from the east in the Amazon basin and the Atlantic. This morphotectonic province creates a topographic barrier to moisture transfer, generating a semiarid climate west of the range (Strecker et al., 2007). Subtropical westerly winds become strong during the austral winter, bringing most of the precipitation (Corripio et al., 2007; Garreaud, 2009). The climate is reversed in the Andes south of 35°S, where summer precipitation and overall moisture is high in the west, with semiarid conditions in the east (Garreaud, 2009).

The geomorphology of the study area consists of glacial, periglacial, and fluvial landforms. Although no ice glaciers lie directly within the study area, late-Pleistocene age glaciation carved out much of the area, leaving behind numerous erosional and depositional forms (Espizua, 2004; Angillieri, 2013). Frost-shattering, solifluction, and ice creep present evidence of ongoing cryogenic processes on the land surface. These processes, coupled with the extreme aridity of the Dry Andes, have allowed ground ice in the form of rock glaciers, protalus ramparts, and other ice-saturated landforms to dominate (Trombotto et al., 1997; Croce and Milana, 2002; Brenning, 2005; Azocar and Brenning, 2010).

Chapter 3

METHODS

3.1 Site Inventory of Rock Glaciers and Periglacial Landforms

A site-specific inventory of rock glaciers and periglacial landforms was compiled by identifying and digitizing the areal extents of 309 ice-rich landforms using high-resolution spaceborne imagery provided by Google Earth. In this region of the Dry Andes, Google Earth imagery is derived from a variety of sources (LandSAT, Digital Globe, and SPOT) draped over global DEM products derived from Shuttle Radar Topography Mission (SRTM) data when in 3D mode (Schmid, 2015).

Landform boundaries were visually defined by breaks in slope, manifested as variations of shading and shadow from topographic relief, and included the landform from the rooting zone to the front slope (e.g., Scotti et al., 2013; Giordino et al., 2014) (Figure 3). In scenarios where multiple landforms converge, the delineation of each landform becomes subjective (Scotti et al., 2013). Our inventory distinguishes each geomorphic body of a distinct origin as its own separate landform. Where converging landform boundaries are indistinguishable, or landforms occur from the same source area on top of one another, we consider the system to be one landform with complex palimpsest features (Figure 4). Rock glaciers and periglacial landforms were visually identified by their unique morphological characteristics such as fretted terrain, elongated furrows, transverse ridges, and coarse debris caps (e.g., Haeberli, 2006; Gruber, 2009).

Talus supply areas for each mapped landform were defined as all areas upslope that visibly appear to be contributing debris to each landform, and included the area from the landform's rooting zone to the peak of the upslope ridge (Figure 3). We subdivided our inventory into three categories. Rock glaciers were separated into two categories based on shape: tongue shaped rock glaciers, which we refer to as "rock glaciers", and lobate shaped rock glaciers, which we refer to as "lobate complexes". Our third category consists of protalus ramparts, which, unlike rock glaciers, do not display indications of flow. Although some studies have further categorized rock glaciers as active, inactive, or relict based on imagery alone (Janke, 2015), we do not make these interpretations so as to avoid inferring ice content without ground-truthing via field investigations (i.e., drilling, geophysical surveying, etc.).

3.2 Extraction of Statistics

Elevation data for each landform were extracted using the 309 landform boundaries to mask the ASTER GDEM (i.e., we masked the elevation grid and extracted only elevation values underlying the polygon features). This process generated a discontinuous DEM of elevation values only within landform boundaries. The GDEM provides elevation data at a 15-m ground sampling distance (GSD) and is publicly available from the U.S. Geological Survey (USGS). From the GDEM, we calculated slope, aspect, solar radiation, and MAGT for each point in the entire region (Figures 5-8). Statistics calculated from the GDEM were confined to each boundary and exported to a statistical analysis package. The 28 variables used in the final multivariate analysis are as follows: periglacial landform (PGL) (1) centroid longitude and (2) latitude in meters of easting and northing within Campo Inchauspe Argentina Zone 2; (3) PGL area reported to the nearest 0.1km^2, (4) PGL perimeter in meters, and (5) the PGL perimeter/area ratio; (6) PGL minimum elevation, (7) maximum elevation, (8) mean elevation, and (9) median elevation; (10) PGL average slope; (11)

PGL north-south and (12) east-west aspect; (13) PGL MAGT minimum, (14) maximum, and (15) mean; (16) talus supply (TS) area reported to the nearest 0.1 km^2, (17) TS perimeter in meters, and (18) the TS perimeter/area ratio; (19) TS minimum elevation, (20) maximum elevation, (21) mean elevation, and (22) median elevation; (23) TS average slope; (24) TS north-south and (25) east-west aspect; (26)TS MAGT minimum, (27) maximum and (28) mean.

3.3 Mean Annual Ground Temperature

Ground temperatures in the study area are known to be dependent on elevation, topography, and insolation (e.g., Bodin et al., 2010; Ruiz and Trombotto Liaudat, 2012; Apaloo et al., 2012). We thus estimated MAGT using previously published methods by our group as follows. First, potential incoming shortwave radiation (PSWR) was calculated for each pixel of the ASTER DEM using the solar analyst toolset in ArcGIS (Schreiber, 2015; Fu and Rich, 1999). This tool considers atmospheric attenuation, site latitude and elevation, slope, aspect, sun angle based on daily and seasonal motion and topography shadows, and bases its calculations on the DEM and adjustable parameters such as atmospheric transmissivity, and diffusion proportion (Huang and Fu, 2009). Next, the MAGT was calculated by modeling the relationship between temperature and elevation, easting, northing, aspect (both north and east components), slope, and solar radiation values (e.g., Schreiber, 2015; Gruber and Hoelzle, 2001; Brenning, 2005) using the following equation:

$$MAGT = a * Z + b * PSWR + c$$

where MAGT is mean annual ground temperature (◦C); Z is land surface elevation (m); PSWR is potential shortwave radiation (W/m^2), the direct insolation variable from the radiation model; and a, b, and c represent site-specific coefficients of the multiple linear regression equation (Schreiber, 2015). This equation was used to generate an estimated MAGT for each cell of the GDEM.

3.4 Multivariate Statistical Analysis

We performed multivariate analyses on the inventory to examine relationships among the aforementioned 28 variables. The variables were first compared against one another by calculating correlation coefficients for the entire inventory, and then among each of the three landform categories (rock glaciers, lobate complexes, protalus ramparts) Pairs of variables that demonstrated correlations with absolute values that exceeded 0.5 were considered to have a high correlation. Next, a principle components analysis (PCA) was performed on the entire inventory and on each landform category individually using the 28 variables to detect linear relationships and to statistically identify which variables or groups of variables best explain variation within the dataset.

Chapter 4

RESULTS

4.1 Summary of the Inventory

A total of 309 landforms indicative of potential ice-saturation were identified in the study area, including 88 rock glaciers, 132 lobate complexes, and 89 protalus ramparts. In March 2017, 79 landforms that are accessible by roads were verified in the field to confirm the accuracy of the inventory. Collectively, these landforms occupy a total area of 55.7 km^2. Smaller landforms are more prevalent with 161 (52.1%) smaller than 0.1 km^2, while 234 (75.7%) are smaller than 0.2 km^2 (Figure 9). Rock glaciers and lobate complexes have a similar size distribution, however protalus ramparts are much smaller with 71% of protalus ramparts smaller than 0.5 km^2. All inventoried landforms are sited above 3105 meters (above sea level), but have an average minimum elevation of 3866 m with 94% above 3600 m (Figure 10). Mean slopes of the individual landforms range from 6° to 33°, with an overall mean slope of 19° (Figure 11). Rock glaciers and lobate complexes are predominantly found on slopes in the 15° to 20° range, where a total of 61% and 54% lie, respectively. Comparatively, protalus ramparts dominate on steeper slopes between 20° and 25°, where 44% of such landforms are found. Talus supply areas reach mean slopes as high as 42°, but no lower than 18°, with a group average of 33°. Of all the landforms in the inventory, 84% have talus slopes with minimum MAGT below 0° C, and 94% of rock glaciers have talus supplies with minimum MAGT below 0° C (Figure 12). South-facing landforms dominate the inventory (239 landforms, or 77.3% in degree range 90° - 270°), while only 70 landforms (22.7%) face to the north (in degree range 270° - 90°, Figure 13). The few landforms that are located on northern (northwest, north, and northeast) facing slopes have mean elevations well above the overall mean, ranging from 3571 to 4564 m (Figure 14). The northern sloping landforms are also found in areas where average talus supply areas reach maximum elevations of 4296 m.

4.2 Multivariate Analyses

Multivariate analyses performed on the entire inventory revealed several high correlations among variables in our dataset (Table 1). Larger periglacial landforms correlate positively with talus supply area altitudinal and size variables, and negatively with talus supply minimum MAGT, suggesting that larger PGL size is encouraged by colder, higher-altitude, larger talus supply areas. Our landform perimeter-to-area ratio, where larger values demonstrate a greater degree of landform elongation, correlated positively with slope and talus supply temperature variables, and negatively with all size variables and talus supply elevation, suggesting that elongation in landforms is encouraged by higher slopes and higher temperatures. Unexpectedly, the two aspect parameters, north-south and east-west, did not correlate highly with any variables other than the talus supply aspect parameters.

The relationships among variables in the individual correlation matrices for each of the three categories of landform were similar to that of the entire inventory, with a few notable differences. High correlations were observed between the altitudinal and temperature variables of the talus supply and size variables among rock glaciers and lobate complexes, but not protalus ramparts (Table 1). High correlations were also observed between north-south aspect and elevation among rock glaciers and lobate complexes (Table 1) but such correlations were not present among protalus ramparts.

A PCA applied to all 28 variables on all 309 landforms produced five components with eigenvalues greater than 1.0, indicating above-average variance explained by those components (Table 2). The first 4 components explain over 85% of the variance in the dataset and have loadings that give insight into the meaning of each component. The first component (PC1) explains the most (over 49%) of variance in the data. PC1 loads high on all elevation and temperature variables. Because the MAGT model is closely linked to the DEM, we interpret this component to represent the altitude of the landforms. The second component (PC2) explains 25% of the variance, with high loadings on all size variables; thus, we interpret PC2 to be indicative of landform size. The third component (PC3) encompasses 8% of the variance in the dataset and represents north-south aspect. The fourth component (PC4) encompasses 5% of the variance in the dataset and represents east-west aspect. For the purposes of our study, we consider PC3 and PC4 together to indicate the importance of orientation on landform formation and persistence.

We repeated the PCA using all 28 variables, but for each landform category separately (rock glaciers, lobate complexes, and protalus ramparts). We then reinterpreted the first three components for each category. PC1 (variance: rock glaciers 49.3%, lobate complexes 45.3%, protalus ramparts 40.7%) and PC2 (variance: rock glaciers 15.1%, lobate complexes 18.1%, protalus ramparts 18.4%) represent altitude and size, respectively, consistent with the first two components from the PCA on the full inventory. On the third component, each landform category reveals different explanations for its dataset variation. For rock glaciers, PC3 (11.6% variance) displays loadings on latitude, slope, aspect, and talus supply mean MAGT, whereas the PC3 for lobate complexes (12.4% variance) and protalus ramparts (12.66% variance) both behave similarly, with loadings on north-south aspects, minimum MAGT, and mean talus supply MAGT. Lobate complexes additionally have a high negative loading on slope for PC3.

Chapter 5

DISCUSSION

Most analyses of ground ice in the Dry Andes focus only on rock glaciers, and no study has yet analyzed the impact that the contributing talus supply has on the formation and distribution of these landforms. The results of this study indicate that the physiographic characteristics of where the landforms are found, as well as the characteristics of each adjacent talus supply area, together play a critical role in where these ice-saturated landforms occur and how they manifest. We find that all of these landforms preferentially occur where large adjacent talus slopes reach high elevations and cold temperatures. However, larger, higher, colder talus supplies favor the formation of rock glaciers. Protalus ramparts dominate over rock glaciers and lobate complexes when adjacent talus supply is smaller, elongated, and at warm, low elevations. Understanding how topographic variation promotes the shape and size of persistent ground ice in this remote environment is critical to preserving valuable water resources while enabling responsible economic growth in these sensitive regions.

An analysis of our inventory of 309 periglacial landforms reveals that size, elevation, and slope all vary between rock glaciers, lobate complexes, and protalus ramparts. As expected, protalus ramparts are overall much smaller in area than rock glaciers and lobate complexes. Rock glaciers and lobate complexes show a similar distribution of individual landform area (with mean areas of 0.26 km^2 and 0.22 km^2), whereas protalus ramparts are commonly much smaller, with an individual landform mean area of 0.04 km^2. All landforms have a strong tendency to form at elevations in the 3700 m to 4000 m range. Lobate complexes and protalus ramparts also have a significant presence at lower elevations, from 3500 m to 3700 m, where rock glaciers are not nearly as common. This suggests that the preferential conditions for rock glacier formation is limited to higher elevations than for that of protalus rampart and/or lobate complex formation. Rock glaciers and lobate complexes are distributed among similar slope conditions (Figure 11), whereas protalus ramparts are found more commonly on steeper slopes where few other landforms are located. It is well known that both exposed glacial ice and ground-ice preferentially occur on slopes oriented to receive the least amount of solar radiation (i.e., poleward) (Angilleri 2009; Scotti et al., 2013). In the northern hemisphere, we see icy landforms oriented to the north, whereas in the southern hemisphere we expect, conversely, to see them dominantly oriented south. Our inventory confirms this. However, surprisingly, 22.7% of the landforms in our study area were located on north-oriented slopes. The north-oriented landforms had mean elevations ranging from 3571 to 4564 m, near or above the overall average mean elevation of 3951 m, suggesting that higher elevations likely compensate for unfavorable solar radiation conditions.

We observed several differences in talus supply characteristics among the three categories of landforms. Rock glaciers and lobate complexes show a similar distribution of adjacent talus supply area size, which ranged from 0.1 km^2 up to 0.5 km^2, whereas protalus ramparts commonly have much smaller talus supplies, limited in area from 0.1 km^2 to 0.2 km^2. The correlation of landform size with talus supply size, combined with observations of talus-supply size suggest that the presence and size of protalus ramparts may be limited to areas adjacent to smaller talus supplies.

Another critical correlation is the distribution of landforms with respect to the minimum MAGT of their adjacent talus supply areas. Rock glaciers and lobate complexes are clearly found in greater abundance at the foot of talus slopes with colder MAGT, whereas protalus ramparts are rare wherever adjacent talus supplies reach minimum MAGT below -4°, but abundant near warmer slopes where talus supplies reach their coldest MAGT of -2° to 2°. We also observe that rock glaciers have much colder talus supplies than protalus ramparts that are located at the same elevation (Figure 15). This evidence indicates that larger, higher, colder talus supplies encourage the formation of rock glaciers and lobate complexes preferentially over protalus ramparts.

Determining and verifying the activity, movement, and ice content of periglacial landforms, and understanding periglacial landform genesis typically requires rigorous field methods that are difficult and expensive to carry out. Field work is especially problematic in remote mountainous terrain such as the Dry Andes, where the pursuit of a field-based inventory as large in scope as ours may very well be impossible. Our investigation was prompted by the findings of studies that suggested that ice content, and therefore the significance of each individual landform as a water resource, could be estimated using remote techniques (Azocar and Brenning, 2010). In general, our inventory suggests that spaceborne imagery presents a promising method to identify numerous landforms that have the potential to hold ice in remote areas where drilling, geophysical surveys, and other field methods are unrealistic. During field work undertaken in March 2017, we verified the presence of 79 of the more easily accessed landforms, a vital and positive test of the reliability of our methods.

Our inventory can thus serve as a foundation for future studies to apply such techniques to gain a better understanding of how rock glaciers and periglacial landforms contribute to local hydrology in the Dry Andes.

FIGURES

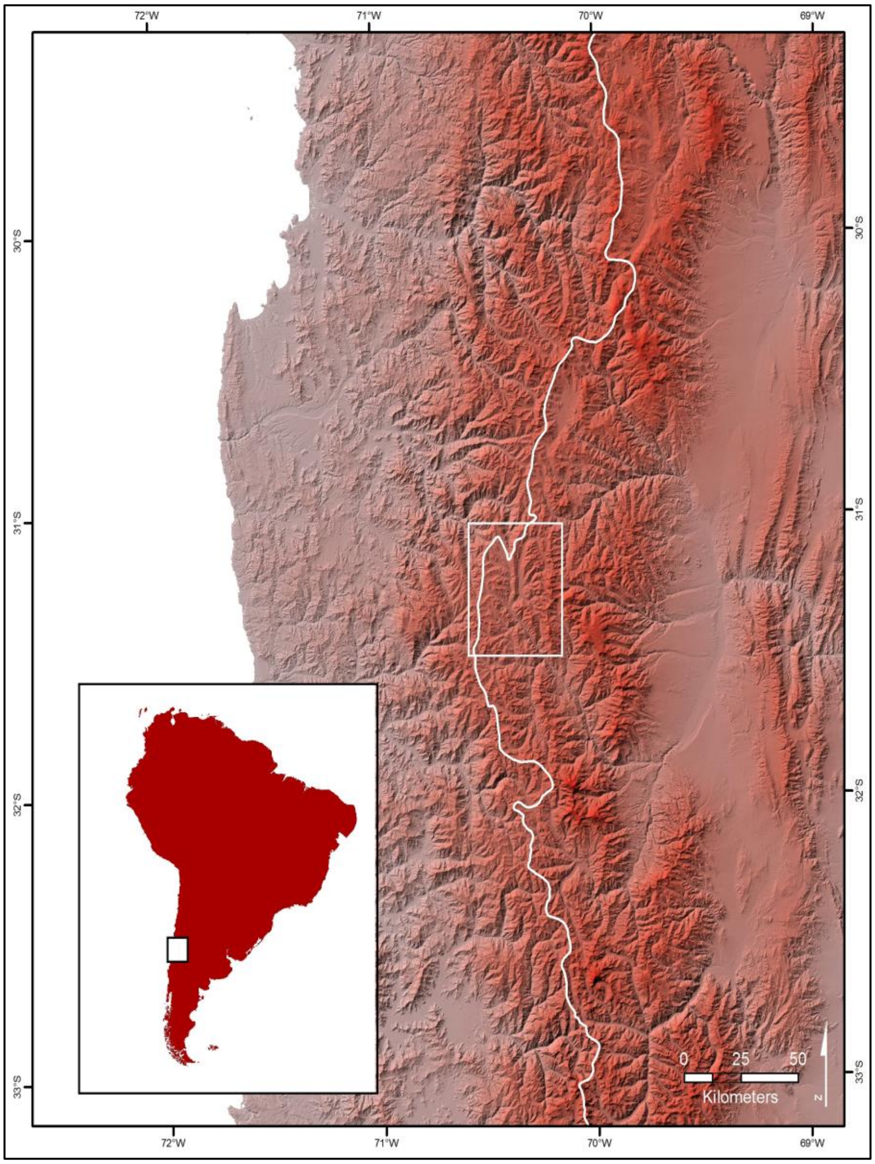

Figure 1: Shaded relief map showing the location of the study area near the Chilean border in the Dry Andes of Argentina with an inset map displaying the area within the context of South America.

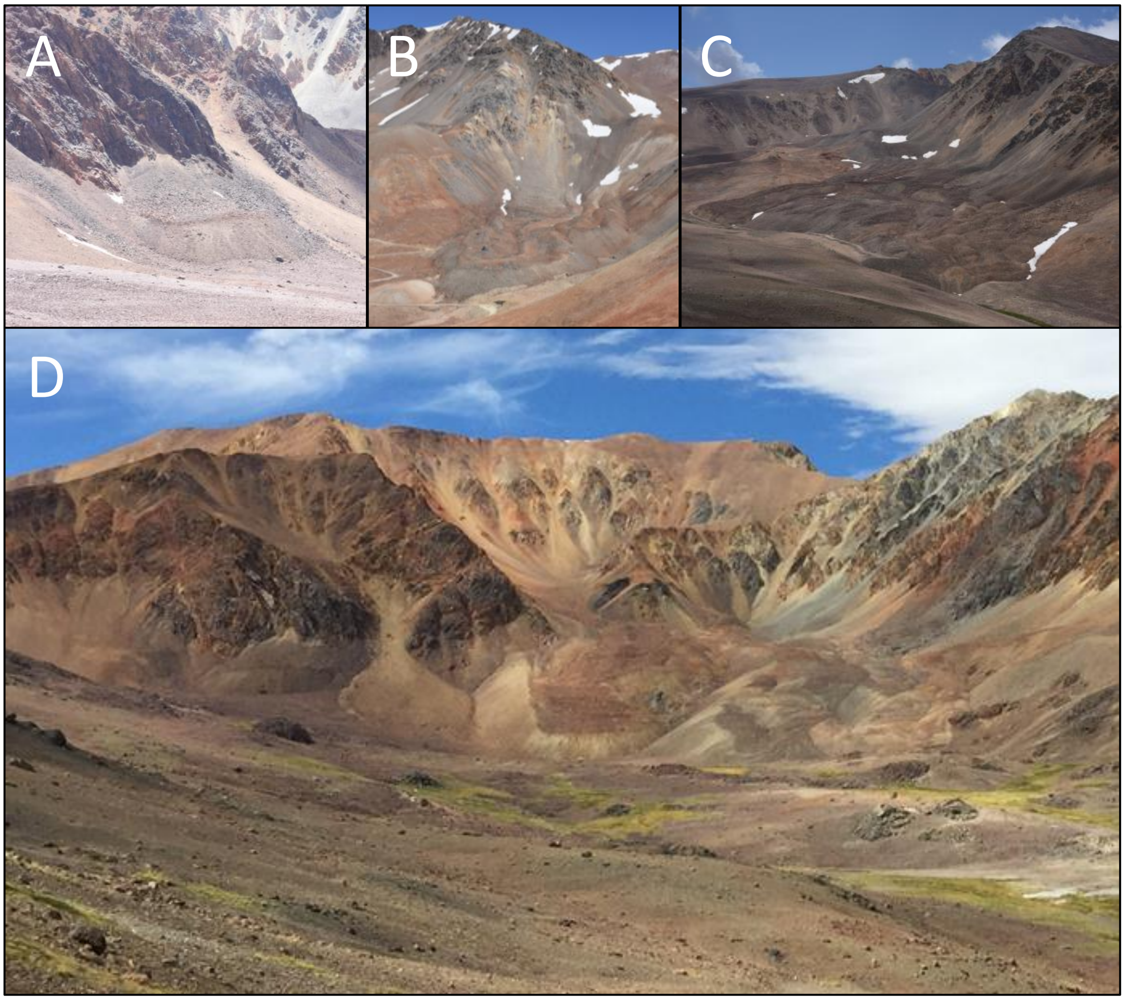

Figure 2: Classification examples. A) Protalus rampart. B) Tongue-shaped rock glacier. C) Lobate rock glacier complex. D) From left to right; a protalus rampart, a simple talus cone, a well-developed rock glacier, and a lobate complex all present under similar physiographic conditions.

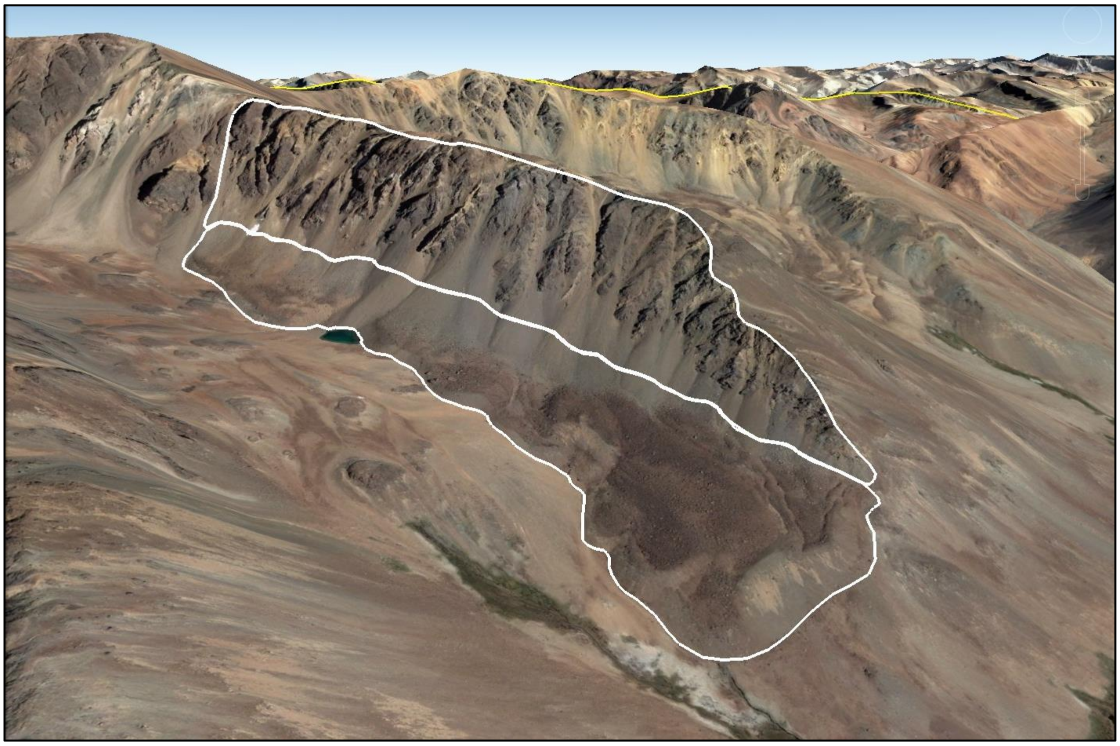

Figure 3: Example of digitized boundaries for a lobate complex and adjacent talus supply area.

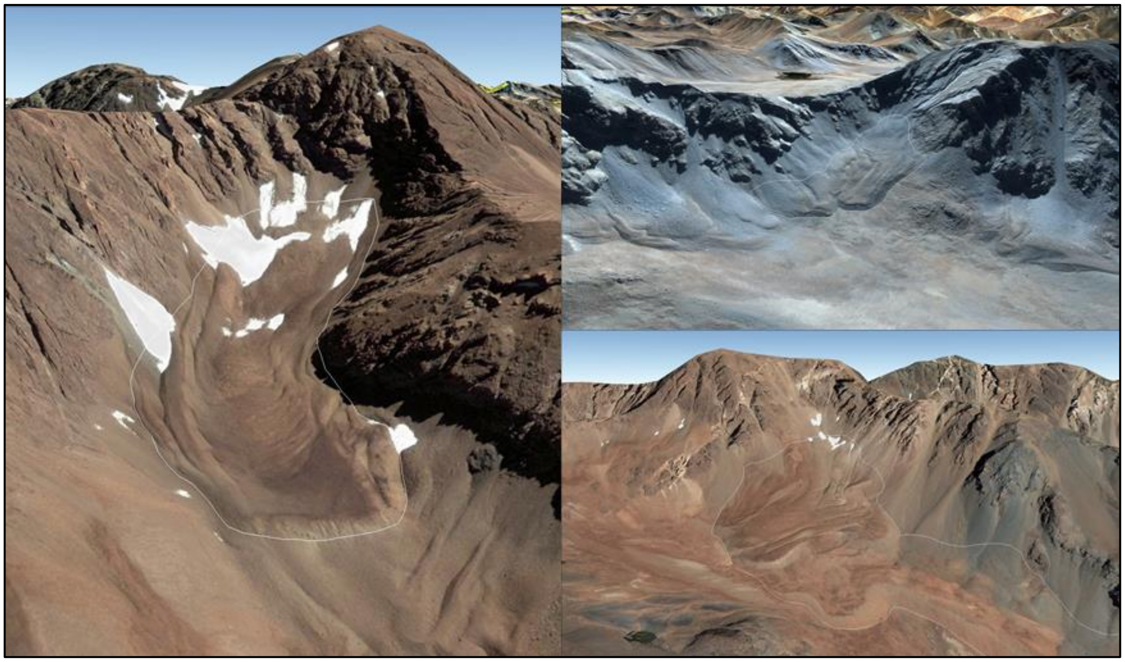

Figure 4: Examples of boundaries showing a) a simple landform with its own distinct origin and boundary, b) a coalescent boundary, where landforms from different origins converge and thus make the boundary between them indistinguishable, and c) a polymorphic boundary, where landforms from the same origin form on top of one another.

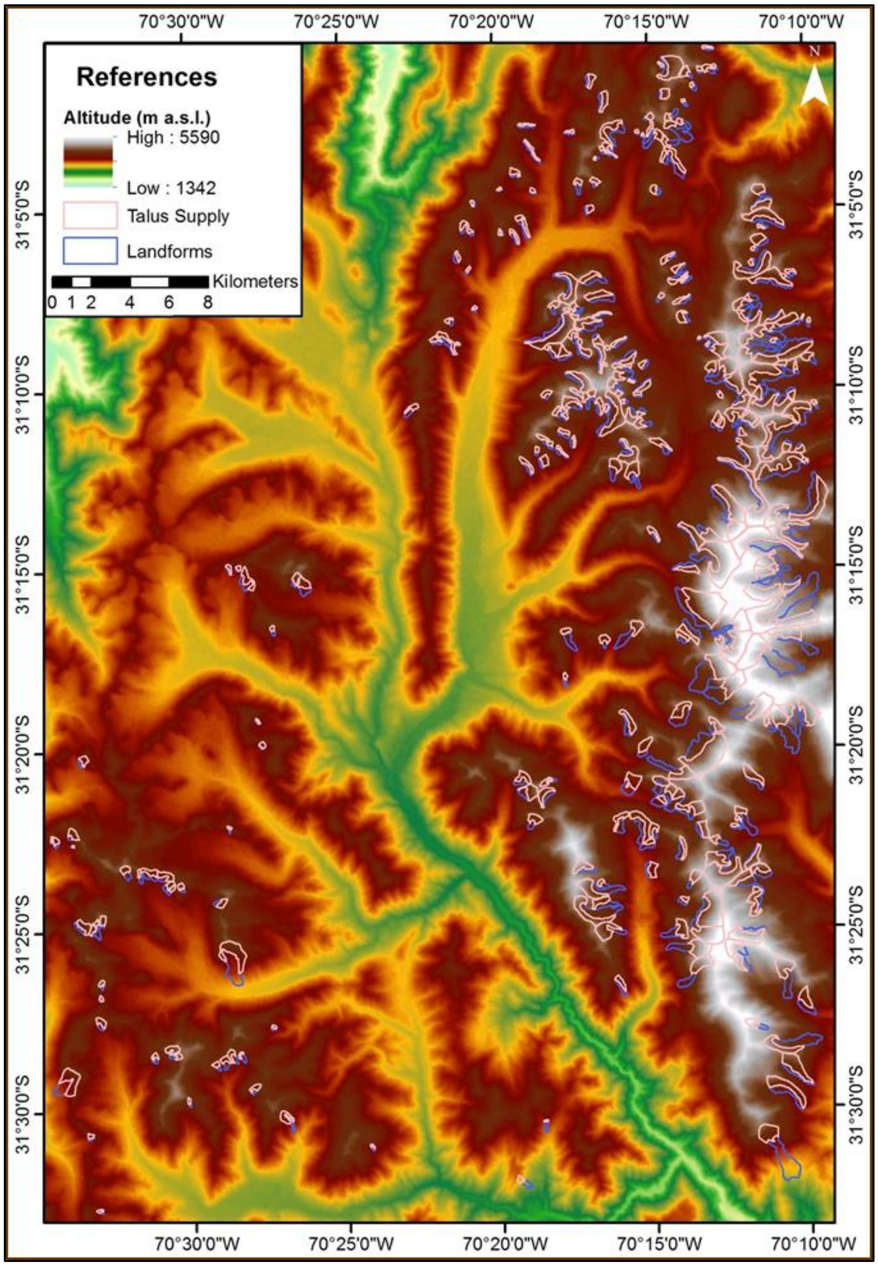

Figure 5: ASTER Global Digital elevation model (GDEM) for the study area with all periglacial landforms and talus supply boundaries overlain.

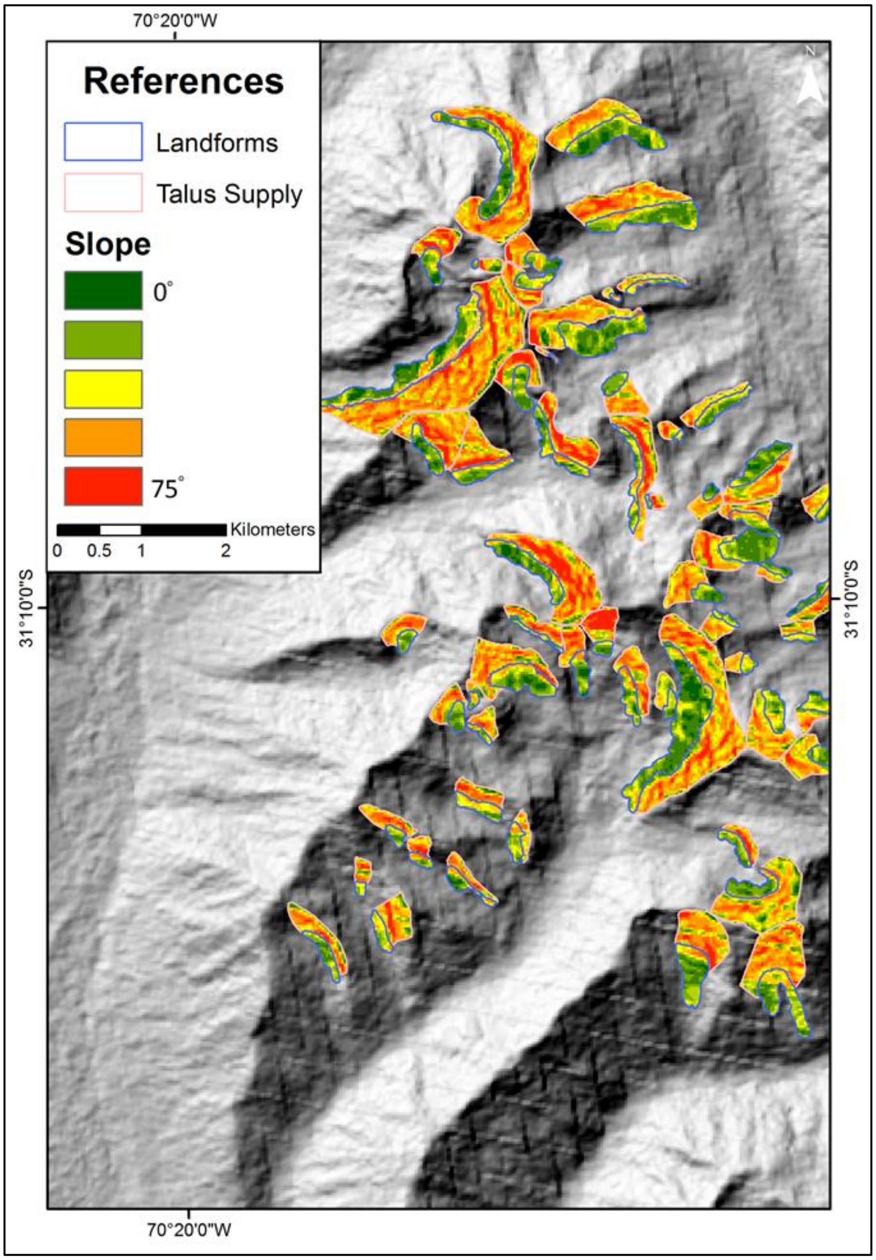

Figure 6: Sample area of landform and talus supply boundaries displaying slope values overlaid on a shaded relief model.

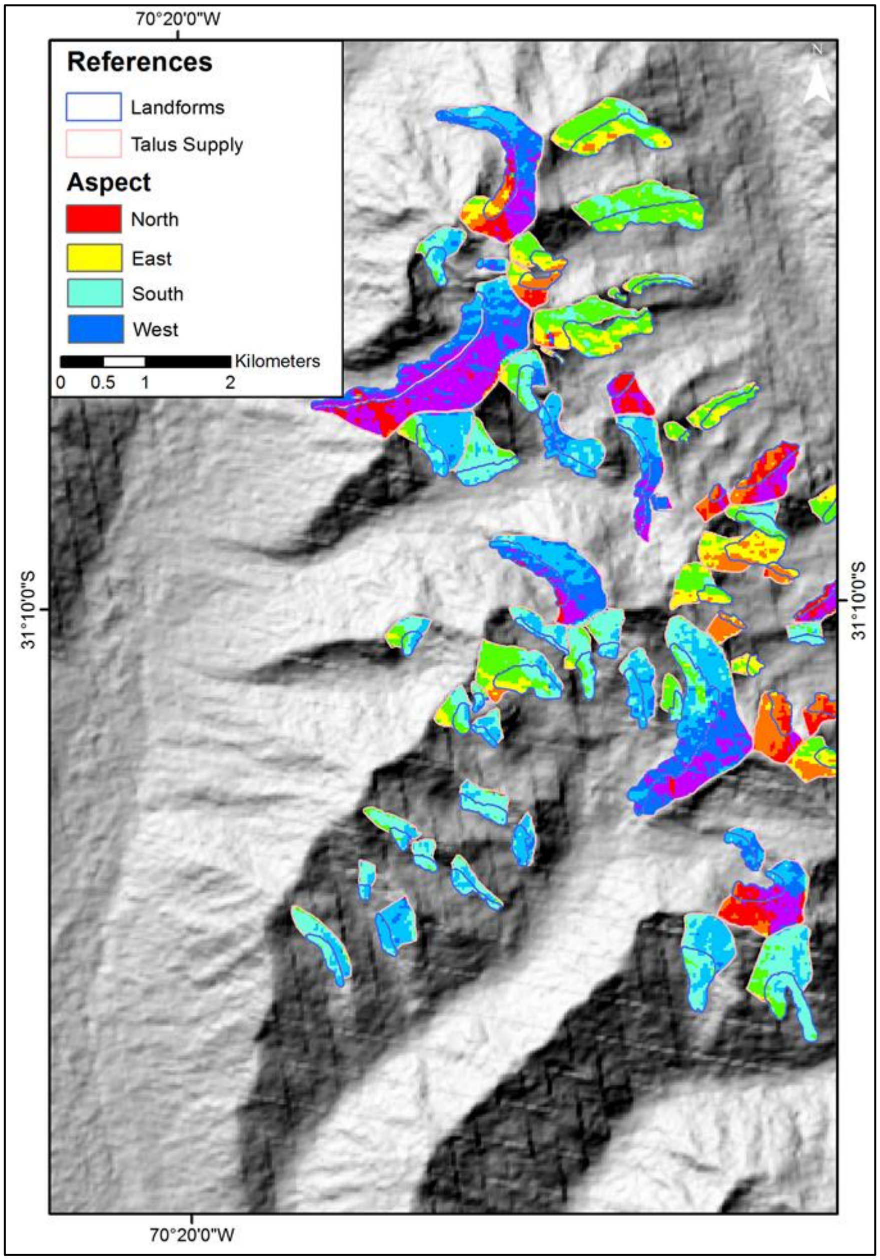

Figure 7: Sample area of landform and talus supply boundaries displaying aspect values overlaid on a shaded relief model.

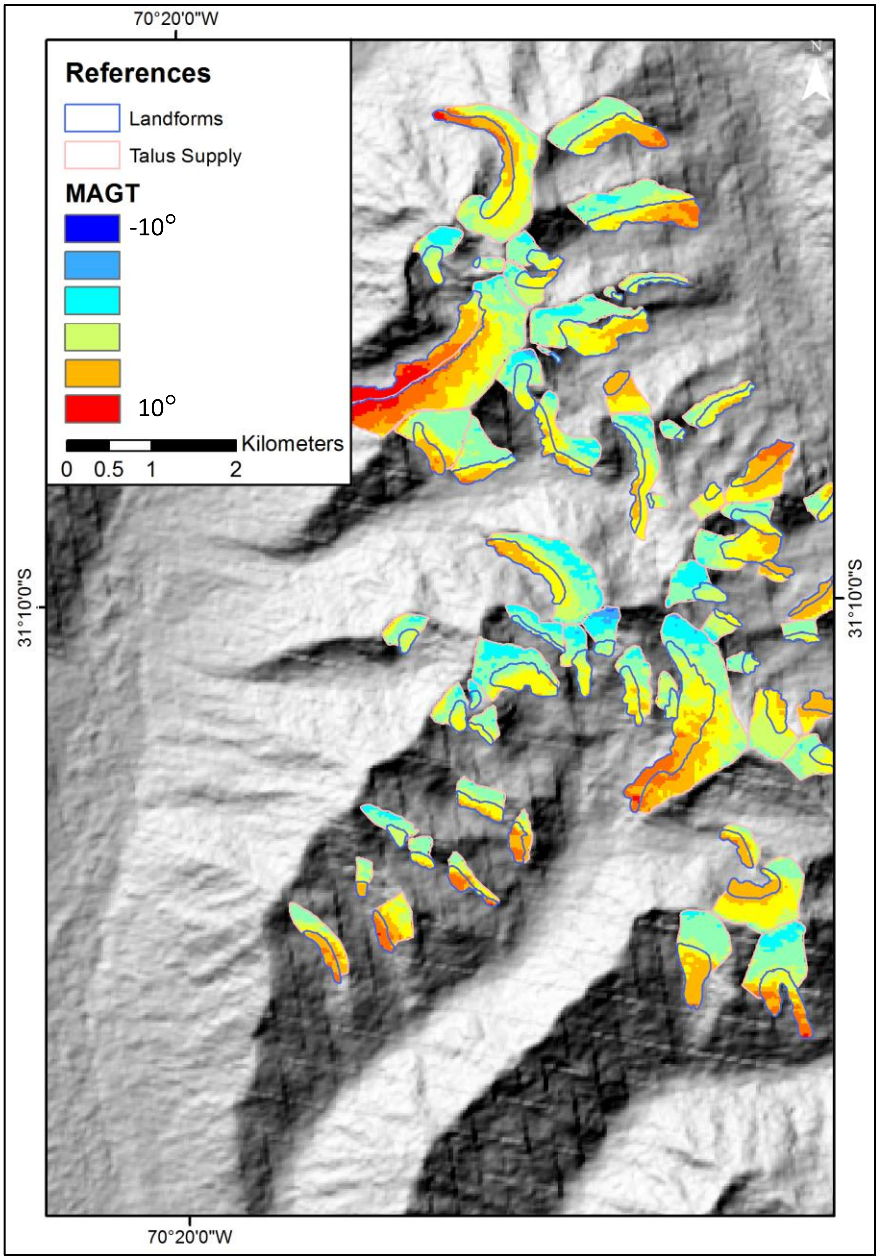

Figure 8: Sample area of landform and talus supply boundaries displaying mean annual ground temperature (MAGT) overlaid on a shaded relief model.

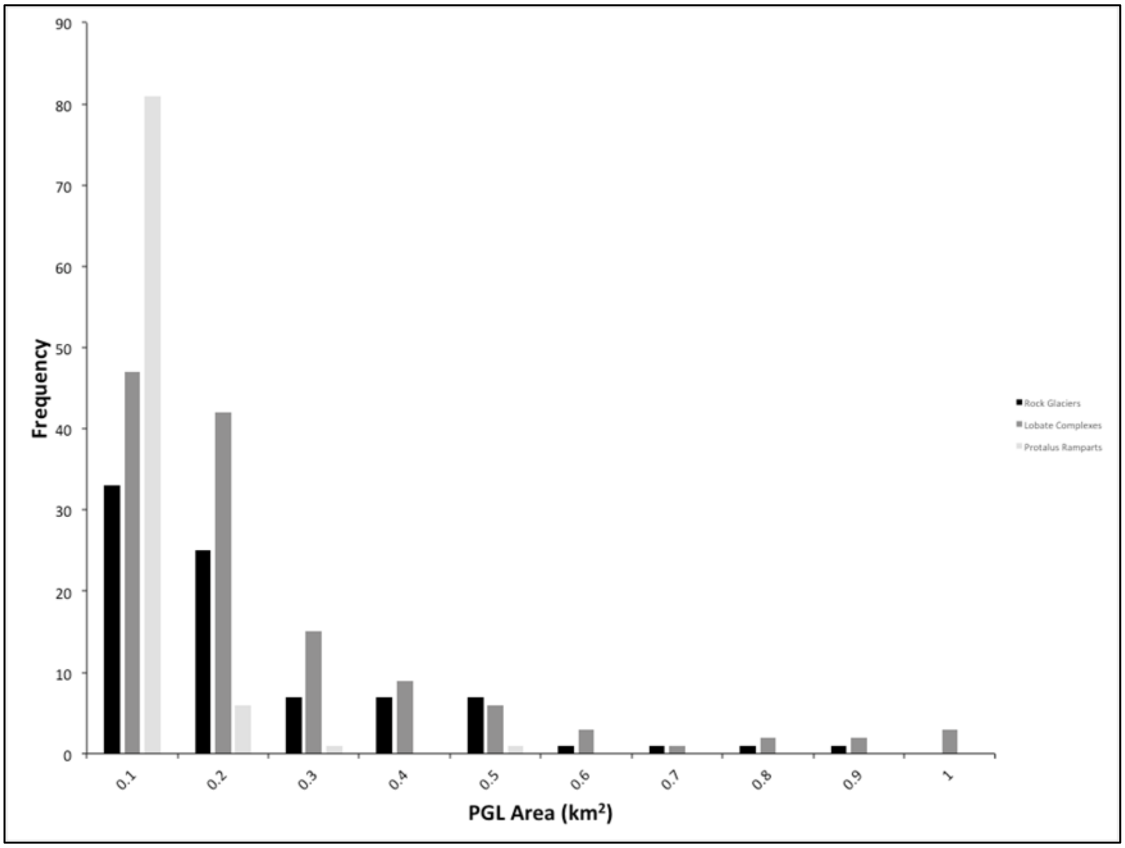

Figure 9: Histogram of periglacial landform area frequencies in 0.1km^2 intervals.

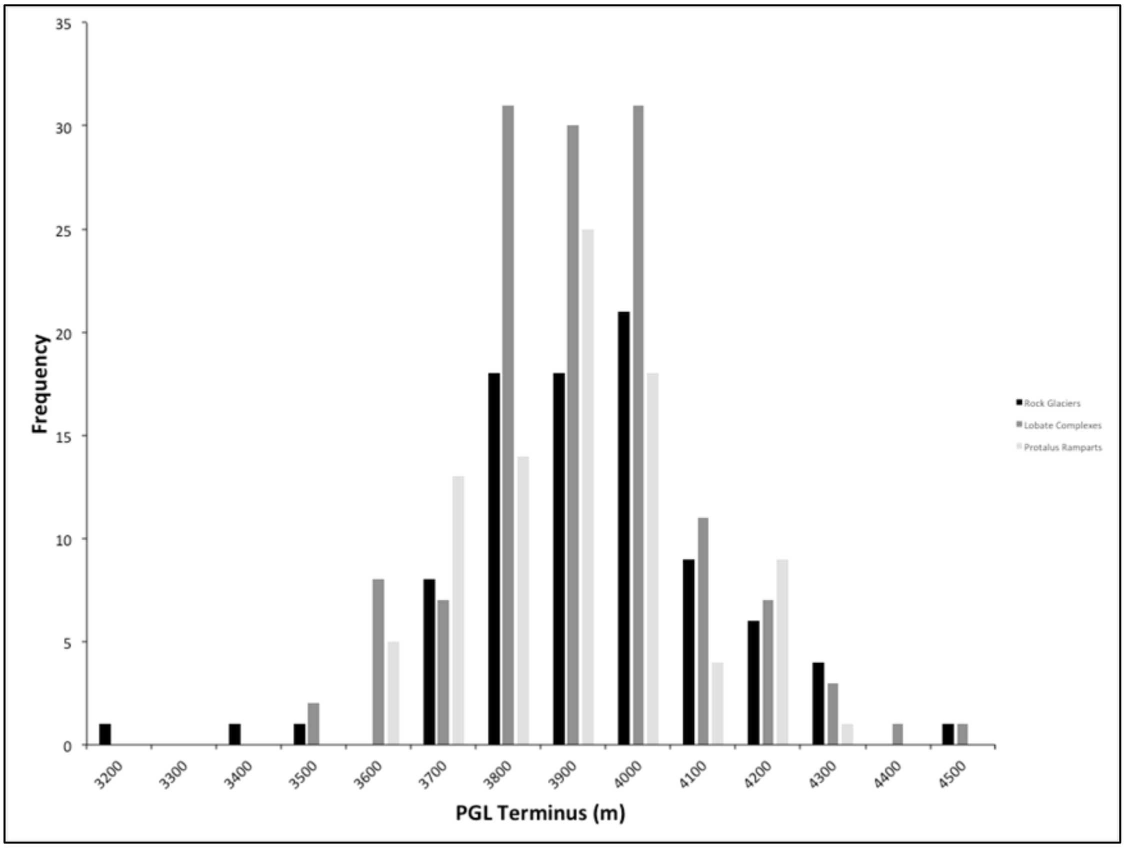

Figure 10: Histogram of periglacial landform minimum elevation frequencies in 100m intervals.

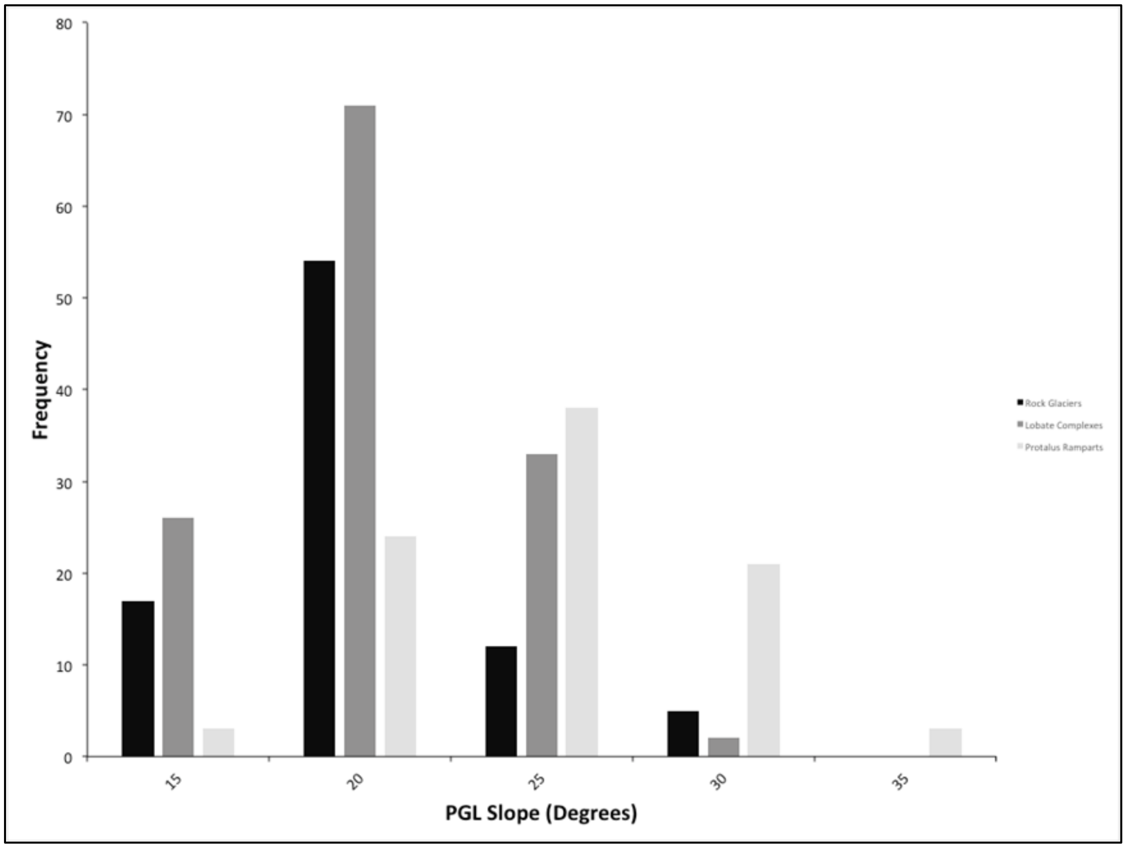

Figure 11: Histogram of periglacial landform mean slope frequencies in 5° intervals.

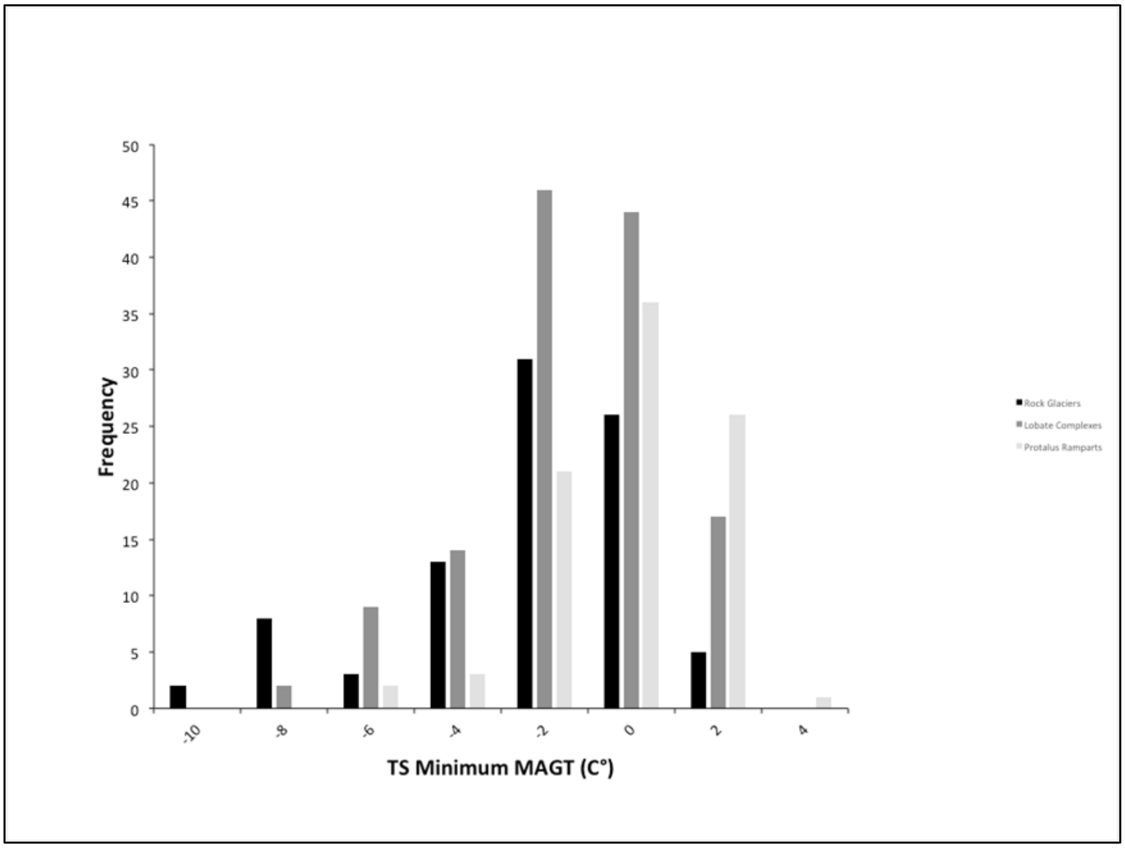

Figure 12: Histogram of talus supply minimum MAGT frequencies in -2° intervals.

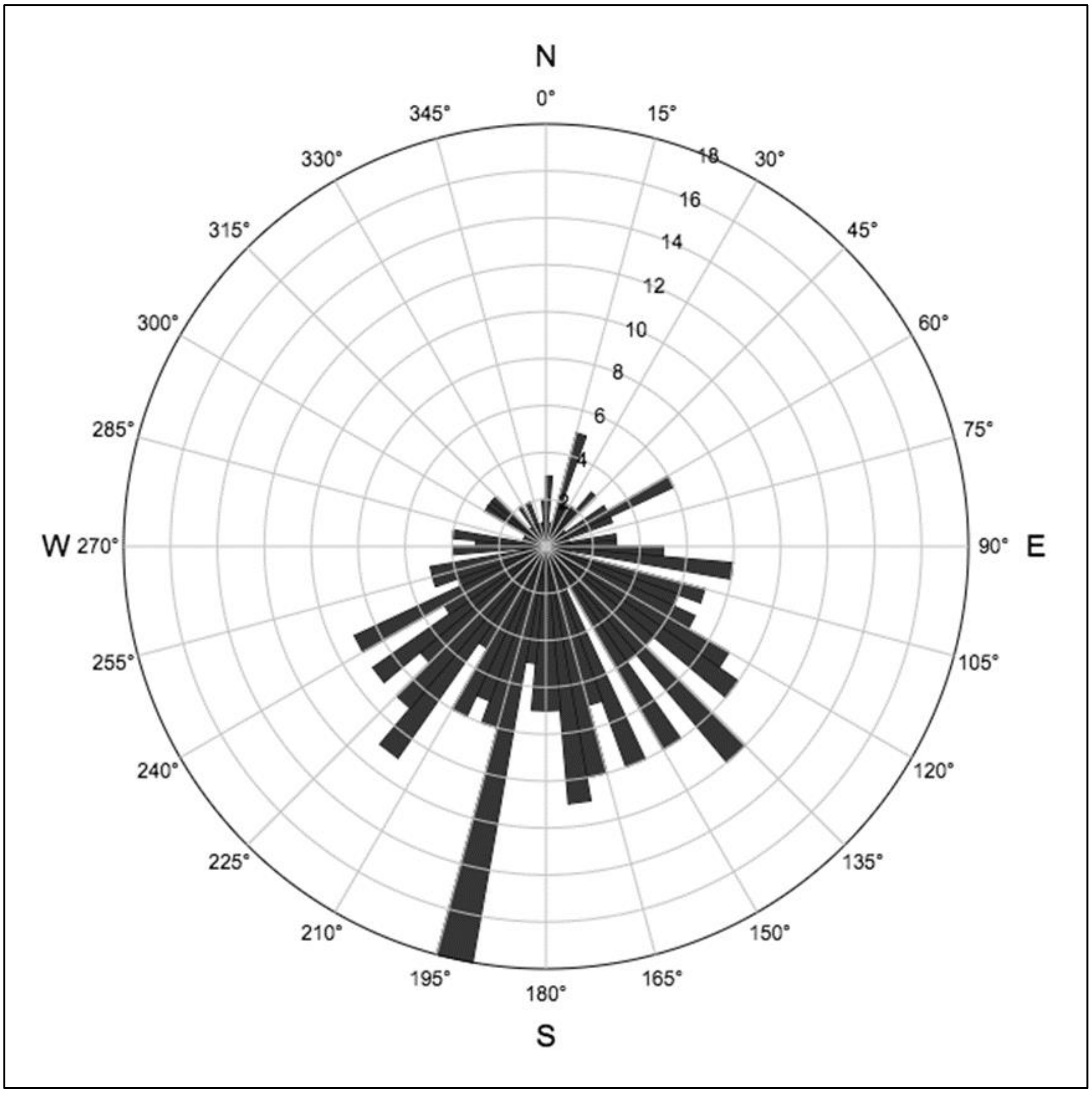

Figure 13: Rose diagram displaying the frequency of periglacial landform mean aspect in 5° intervals.

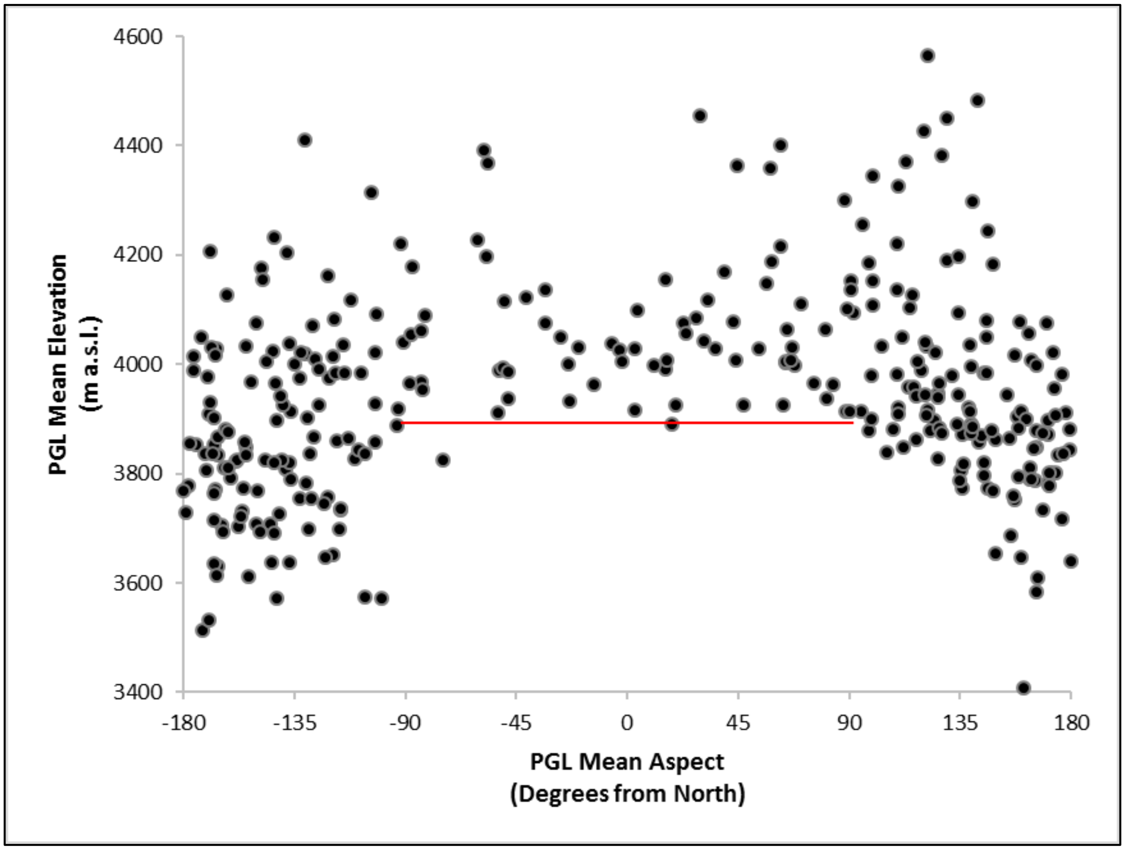

Figure 14: Periglacial landform elevation plotted against mean aspect. The overall mean elevation of the inventory (3894 m) is marked, demonstrating that nearly all north-oriented landforms are situated well above the overall mean.

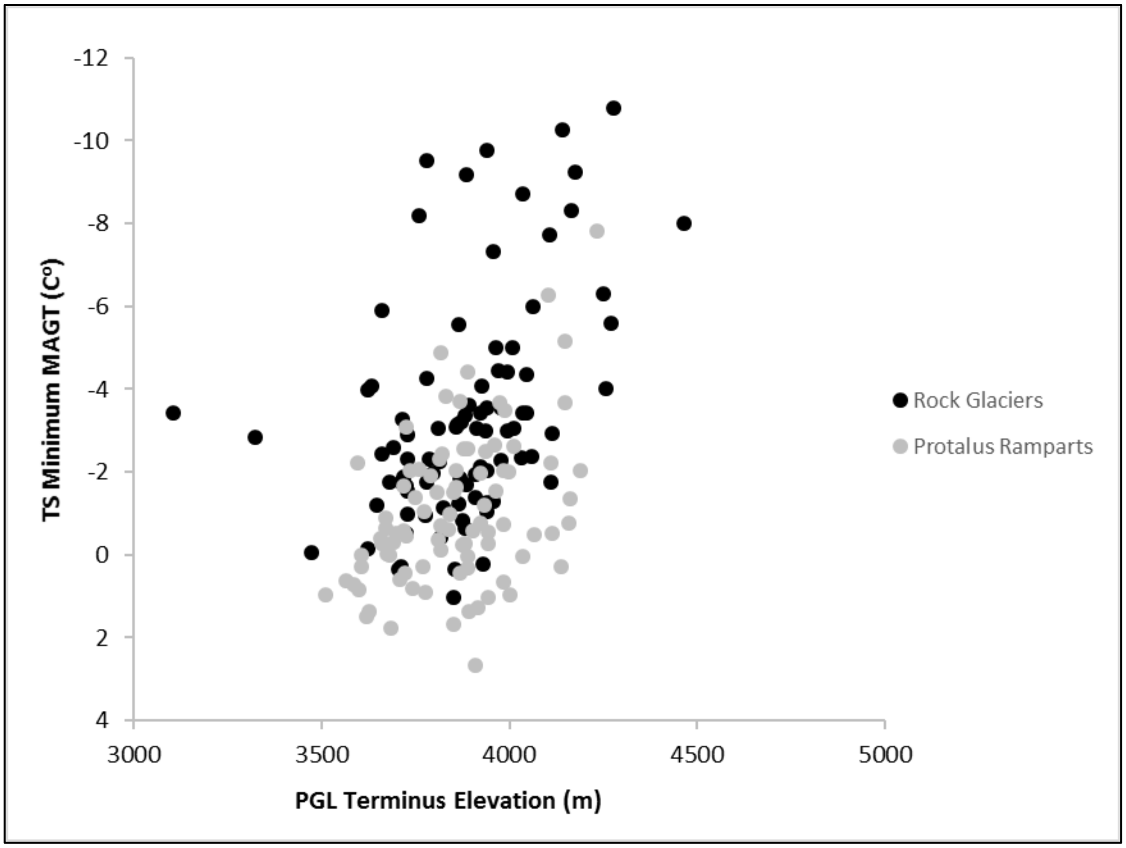

Figure 15: Rock glacier and protalus rampart minimum elevation plotted against talus supply minimum MAGT. Rock glaciers have much colder talus supply areas than protalus ramparts located at similar elevations.

TABLES

	PGL LONGITUDE	PGL LATITUDE	PGL AREA	PGL PERIMETER	PGL Perimeter:Area	PGL Minimum Elevation	PGL Maximum Elevation	PGL Mean Elevation	PGL Median Elevation	PGL Slope	PGL East-West Aspect	PGL North-South Aspect	PGL Minimum MAGT	PGL Maximum MAGT
PGL LATITUDE	0.3919													
PGL AREA	0.2784	-0.1833												
PGL PERIMETER	0.3376	-0.1293	0.8848											
PGL Perimeter:Area	-0.3134	0.2319	-0.5685	-0.6128										
PGL Minimum Elevation	0.4306	0.2378	-0.0653	-0.0696	0.0119									
PGL Maximum Elevation	0.556	0.0351	0.4536	0.4865	-0.3808	0.7893								
PGL Mean Elevation	0.5213	0.1397	0.2168	0.2355	-0.196	0.9397	0.9477							
PGL Median Elevation	0.5199	0.1425	0.2128	0.2367	-0.1935	0.9372	0.9442	0.9989						
PGL Slope	-0.3568	-0.0372	-0.3955	-0.4522	0.5282	-0.2129	-0.3865	-0.3203	-0.3219					
PGL East-West Aspect	0.2248	0.1364	0.055	0.0168	-0.0677	0.1972	0.1915	0.2023	0.2022	-0.2385				
PGL North-South Aspect	0.3549	0.1006	0.217	0.2744	-0.196	0.3669	0.4296	0.4288	0.431	-0.4309	0.0988			
PGL Minimum MAGT	-0.3715	0.0717	-0.4511	-0.4625	0.3814	-0.5428	-0.7937	-0.7062	-0.7024	0.161	-0.1376	0.0928		
PGL Maximum MAGT	-0.2501	-0.2013	0.2138	0.2425	-0.1922	-0.8963	-0.6239	-0.798	-0.796	-0.0554	-0.1154	-0.0043	0.5559	
PGL Mean MAGT	-0.32	-0.0834	-0.0666	-0.0545	0.0278	-0.821	-0.7688	-0.8391	-0.8366	-0.0212	-0.1105	0.0958	0.8157	0.9087
TS Area	0.2946	-0.159	0.7526	0.8105	-0.5061	0.1349	0.546	0.3731	0.3731	-0.3828	-0.1109	0.3025	-0.4579	0.008
TS Perimeter	0.3126	-0.138	0.7446	0.8939	-0.576	0.1043	0.5615	0.3684	0.3731	-0.4389	-0.0686	0.3236	-0.4956	0.054
TS Perimeter:Area	-0.237	0.2219	-0.4541	-0.5444	0.7289	-0.0983	-0.4061	-0.2714	-0.272	0.4776	0.1334	-0.2683	0.3349	-0.0659
TS Minimum Elevation	0.5038	0.1108	0.1818	0.1224	-0.1796	0.9051	0.8803	0.9393	0.933	-0.2699	0.1926	0.3771	-0.6597	-0.7716
TS Maximum Elevation	0.5104	-0.105	0.5551	0.5682	-0.5124	0.6138	0.8925	0.7988	0.794	-0.432	0.0281	0.3816	-0.722	-0.4488
TS Mean Elevation	0.5314	-0.0269	0.4512	0.443	-0.4143	0.7548	0.9476	0.9011	0.8954	-0.3851	0.0839	0.4007	-0.7529	-0.5963
TS Median Elevation	0.528	-0.0238	0.4512	0.4462	-0.4122	0.7522	0.948	0.9004	0.8948	-0.3828	0.0787	0.4	-0.7545	-0.5948
TS Slope	0.0014	-0.1834	0.1525	0.1431	-0.262	0.0573	0.147	0.105	0.1007	-0.0589	-0.0111	-0.0261	-0.2077	-0.092
TS East-West Aspect	0.1287	0.1211	-0.0152	-0.0631	-0.0008	0.1416	0.1017	0.1231	0.1217	-0.1736	0.9229	-0.0007	-0.0884	-0.0953
TS North-South Aspect	0.3311	0.1253	0.178	0.2347	-0.1564	0.3737	0.416	0.4252	0.4277	-0.4041	0.0816	0.929	0.0911	-0.0421
TS Minimum MAGT	-0.3365	0.1861	-0.5508	-0.5386	0.5135	-0.4254	-0.7279	-0.6091	-0.6029	0.2877	0.0123	0.0463	0.8239	0.4033
TS Maximum MAGT	-0.3191	-0.0073	-0.0646	0.0208	0.0751	-0.6843	-0.6397	-0.6909	-0.6814	0.0208	-0.1159	0.0942	0.6566	0.7443
TS Mean MAGT	-0.3207	0.1297	-0.3701	-0.3261	0.3655	-0.5221	-0.703	-0.643	-0.6349	0.1575	-0.0483	0.1728	0.8307	0.5718

	PGL Mean MAGT	TS Area	TS Perimeter	TS Perimeter:Area	TS Minimum Elevation	TS Maximum Elevation	TS Mean Elevation	TS Median Elevation	TS Slope	TS East-West Aspect	TS North-South Aspect	TS Minimum MAGT	TS Maximum MAGT
PGL LATITUDE													
PGL AREA													
PGL PERIMETER													
PGL Perimeter:Area													
PGL Minimum Elevation													
PGL Maximum Elevation													
PGL Mean Elevation													
PGL Median Elevation													
PGL Slope													
PGL East-West Aspect													
PGL North-South Aspect													
PGL Minimum MAGT													
PGL Maximum MAGT													
PGL Mean MAGT													
TS Area	-0.2151												
TS Perimeter	-0.1914	0.9124											
TS Perimeter:Area	0.0988	-0.551	-0.6098										
TS Minimum Elevation	-0.798	0.2572	0.2037	-0.2343									
TS Maximum Elevation	-0.6276	0.7194	0.6718	-0.5945	0.7735								
TS Mean Elevation	-0.7347	0.5919	0.5465	-0.4955	0.8958	0.9662							
TS Median Elevation	-0.7349	0.5936	0.5507	-0.4965	0.8919	0.9623	0.9992						
TS Slope	-0.1576	0.1725	0.1389	-0.3345	0.1314	0.3086	0.2411	0.2329					
TS East-West Aspect	-0.0808	-0.1923	-0.1525	0.206	0.1468	-0.0445	0.0121	0.0062	-0.0866				
TS North-South Aspect	0.0634	0.2791	0.303	-0.2484	0.3812	0.3708	0.3978	0.3984	-0.0598	0.0264			
TS Minimum MAGT	0.6616	-0.652	-0.6079	0.5589	-0.6044	-0.8672	-0.8165	-0.8135	-0.3911	0.0472	0.0711		
TS Maximum MAGT	0.8129	-0.1228	-0.0372	0.127	-0.7885	-0.6052	-0.7032	-0.6999	-0.3309	-0.101	0.1138	0.6503	
TS Mean MAGT	0.7857	-0.4441	-0.3854	0.4094	-0.6779	-0.7848	-0.7912	-0.7886	-0.4324	-0.019	0.2041	0.9314	0.8319

Table 1: Correlation matrix displaying the significant statistical correlations among 28 variables pertaining to the 309 periglacial landforms. Green indicates positive correlations greater than 0.5, red indicates negative correlations greater than 0.5, and blue highlights positive correlations greater than 0.8

	Component 1				Component 2				Component 3				Component 4			
	ALL	RG	LC	PR	ALL	RG	LC	PR	ALL	RG	LC	PR	ALL	RG	LC	PR
Eigenvalue	12.8185	13.8071	12.6793	11.3887	4.7779	4.2287	5.0676	5.1525	3.0489	3.2471	3.4631	3.5448	1.962	1.757	1.8658	2.0627
Variance Explained (%)	45.78	49.311	45.283	40.674	17.064	15.103	18.098	18.402	10.889	11.597	12.368	12.66	7.007	6.275	6.663	7.367
PGL LONGITUDE	0.1565	0.15028	0.16096	0.155	0.00811	0.0185	-0.01915	0.02896	0.19727	0.18658	0.16398	0.19642	0.09401	-0.206	0.11818	0.14641
PGL LATITUDE	0.00067	-0.00931	-0.06776	0.06634	-0.14238	-0.13707	-0.10205	-0.11872	0.23018	0.21795	0.18159	0.19556	0.03016	-0.11759	0.03633	0.29538
PGL AREA	0.13718	0.12515	0.14475	0.06735	0.3124	0.36481	0.31192	0.3715	-0.043	0.00359	-0.0019	-0.06646	0.13911	-0.15551	0.21644	0.2318
PGL PERIMETER	0.14087	0.142	0.13758	0.0728	0.34653	0.37048	0.34581	0.3566	-0.00905	0.04366	-0.02522	-0.00711	0.10188	-0.13927	0.17975	0.32533
PGL Perimeter:Area	-0.12717	-0.14114	-0.15987	-0.02574	-0.28397	-0.29819	-0.25879	-0.26606	0.03829	-0.10596	0.01973	0.15279	-0.14849	0.15279	-0.06367	0.20795
PGL Minimum Elevation	0.21248	0.20042	0.21245	0.26296	-0.2501	-0.29316	-0.23526	-0.13854	0.1415	0.09801	0.15166	0.14031	-0.09441	0.10127	-0.12051	-0.05988
PGL Maximum Elevation	0.27015	0.2624	0.26901	0.28083	-0.02505	-0.04197	-0.02037	0.01012	0.07336	0.0576	0.08133	0.1089	-0.00263	0.00476	0.03313	0.07743
PGL Mean Elevation	0.25575	0.24451	0.25774	0.27889	-0.13946	-0.17377	-0.127	-0.05811	0.11608	0.08537	0.12749	0.12991	-0.05457	0.06125	-0.04568	0.01793
PGL Median Elevation	0.25465	0.24241	0.25692	0.27905	-0.13837	-0.17768	-0.12348	-0.0525	0.11915	0.08857	0.13021	0.13061	-0.056	0.06367	-0.04253	0.02356
PGL Slope	-0.11673	-0.08552	-0.10531	-0.08353	-0.1853	-0.12287	-0.13857	-0.17599	-0.22286	-0.33673	-0.28647	-0.11997	-0.15754	0.13458	-0.13767	0.26486
PGL East-West Aspect	-0.03939	-0.01647	0.03726	0.06266	-0.09168	-0.09132	-0.16219	-0.17109	0.19776	0.38786	0.1578	0.06366	0.61413	-0.42228	0.59733	0.05512
PGL North-South Aspect	0.09723	0.13138	0.07787	0.0647	0.10697	0.01655	0.11668	0.141	0.45732	0.35157	0.4607	0.45218	-0.19139	0.31713	-0.1591	-0.16733
PGL Minimum MAGT	-0.22899	-0.23339	-0.21816	-0.21228	0.03126	0.0275	0.02623	0.05651	0.20398	0.11926	0.22852	0.25723	-0.12858	0.17445	-0.14932	-0.26506
PGL Maximum MAGT	-0.17241	-0.1708	-0.17974	-0.22984	0.32986	0.34402	0.30424	0.23669	0.03539	0.05092	0.03505	0.05531	0.08723	-0.05818	0.13705	-0.04185
PGL Mean MAGT	-0.217	-0.21821	-0.22204	-0.23695	0.23542	0.23409	0.21121	0.1729	0.15062	0.12203	0.17165	0.16796	0.00754	0.03219	0.00885	-0.16329
TS Area	0.17248	0.18801	0.16319	0.12361	0.28444	0.26657	0.2913	0.35202	-0.03832	-0.01463	-0.04466	-0.05067	-0.06347	0.18356	0.0175	0.19678
TS Perimeter	0.16799	0.18276	0.16379	0.11961	0.30892	0.27992	0.31967	0.35657	-0.0077	0.03306	-0.0333	-0.04476	-0.02137	0.16516	0.07038	0.2403
TS Perimeter:Area	-0.1421	-0.16538	-0.15401	-0.06865	-0 26048	-0.21049	-0.24852	-0.28216	0.05016	-0.02681	0.06534	0.0878	0.07093	-0.01696	0.12088	0.32453
TS Minimum Elevation	0.24458	0.24592	0.23329	0.26978	-0.17118	-0.14649	-0.19149	-0.11665	0.08723	0.04914	0.13007	0.10793	-0.04201	-0.01756	-0.08084	-0.11309
TS Maximum Elevation	0.26593	0.25951	0.26498	0.2689	0.08203	0.07879	0.07703	0.14295	-0.01915	-0.03903	-0.00287	0.0009	-0.05715	0.04233	-0.05234	-0.11479
TS Mean Elevation	0.27377	0.26521	0.27572	0.28625	-0.00681	0.00433	-0.01746	0.04147	0.0181	-0.00908	0.04432	0.04657	-0.06159	0.05165	-0.06483	-0.10447
TS Median Elevation	0.27339	0.26471	0.27555	0.28575	-0.00587	0.00528	-0.01511	0.04356	0.01818	-0.00828	0.0433	0.04561	-0.06526	0.06008	-0.06543	-0.0955
TS Slope	0.07388	0.09839	0.09536	-0.00355	0.05452	-0.08656	0.08778	0.07946	-0.20935	-0.24962	-0.19837	-0.18797	0.0126	-0.21348	-0.09109	-0.40157
TS East-West Aspect	0.0161	-0.03957	0.00981	0.03618	-0.11476	-0.11437	-0.19248	-0.1715	0.17038	0.34617	0.11973	0.07054	0.62164	-0.43725	0.59715	0.07356
TS North-South Aspect	0.09363	0.12036	0.07686	0.05647	0.08879	-0.02707	0.10983	0.12673	0.46444	0.36525	0.46114	0.45157	-0.20156	0.37522	-0.17615	-0.14583
TS Minimum MAGT	-0.23484	-0.23272	-0.22914	-0.21154	-0.07538	-0.103	-0.06972	-0.05675	0.25451	0.19602	0.25968	0.31743	-0.05456	0.11668	-0.05191	0.10537
TS Maximum MAGT	-0.1969	-0.20526	-0.1908	-0.21912	0.21863	0.1449	0.24879	0.1732	0.18529	0.19673	0.14656	0.18361	-0.03255	0.17138	0.03588	0.13582
TS Mean MAGT	-0.22718	-0.22706	-0.22047	-0.21917	0.0486	-0.01304	0.07576	0.03319	0.29632	0.24199	0.30129	0.32039	-0.08234	0.19155	-0.04729	0.11361

Table 2: Characteristics of the first four components from the PCA. Loadings are shown for each of the 28 variables.

REFERENCES

Apaloo, J., Brenning, A., and Bodin, X. (2012). Interactions between seasonal snow cover, ground surface temperature and topography (Andes of Santiago, Chile, 33.5◦S). Permafrost and Periglacial Processes, 23(4):277–291.

Angillieri, E. (2009). A preliminary inventory of rock glaciers at 30°S latitude, Cordillera Frontal of San Juan, Argentina. Quaternary International. 195: 151-157.

Angillieri, E. (2013). Geomorphological of a portion of the Andes and Pre-Andes of San Juan, Argentina. Journal of Maps. 9(3): 353-360.

Azócar, G. F. and Brenning, A. (2010). Hydrological and geomorphological significance of rock glaciers in the dry Andes, Chile (27-33S). Permafrost and Periglacial Processes, 21(1):42–53.

Ballantyne, C. and Benn, D. (1994) Glaciological Constraints on Protalus Rampart Development. Permafrost and Periglacial Processes, 5: 145-153.

Barsch, D., (1996). Rock glaciers. Indicators for the present and former geoecology in high mountain environments. Springer, Berlin.

Bodin, X., Rojas, F., Brenning, A. (2010). Status and evolution of the cryosphere in the Andes of Santiago (Chile, 33.5°S.). Geomorphology, 118: 453–464.

Brazier, V., Kirkbride, M., Owens, I., (1998). The relationship between climate and rock glacier distribution in the Ben Ohau Range, New Zealand. Geografiska Annaler, 80A (3–4): 193–207.

Brenning, A. (2005). Geomorphological, hydrological and climatic significance of rock glaciers in the Andes of Central Chile (33-35S). Permafrost and Periglacial Processes, 16(3):231–240.

Brenning, A., Grasser, M., Friend, D. (2007). Statistical estimation and generalized additive modeling of rock glacier distribution in the San Juan Mountains, Colorado, United States. Journal of Geophysical Research, 112: F02S15.

Brenning, A. (2010). The significance of rock glaciers in the dry Andes - reply to L. Arenson and M. Jakob. Permafrost and Periglacial Processes, 21(3):286–288.

Corripio, J. G., Purves, R. S., and Rivera, A. (2007). Modelling climate-change impacts on mountain glaciers and water resources in the Central Dry Andes. In Darkening Peaks: Glacier Retreat, Science, and Society, pages 126–135. University of California Press.

Cristallini, E. O., and Ramos, V. A, (2000). Thick-skinned and thin-skinned thrusting in the La Ramada fold and thrust belt: Crustal evolution of the High Andes of San Juan, Argentina (32°S). Tectonophysics, 317: 205-235.

Croce, F. A. and Milana, J. P. (2002). Internal structure and behaviour of a rock glacier in the arid Andes of Argentina. Permafrost and Periglacial Processes, 13(4):289–299.

Espizua, L. E. (2004). Pleistocene glaciations in the Mendoza Andes, Argentina. Quaternary Glaciations Extent and Chronology Part III: South America, Asia, Africa, Australasia, Antarctica, volume 2, Part C of Developments in Quaternary Sciences, pages 69 – 73.

Falaschi, D., Castro, M., Masiokas, M., Tadono, T., Ahumada, A. (2014). Rock Glacier Inventory of the Valles Calchaquies Region (~25°S), Salta, Argentina Derived from ALOS Data. Permafrost and Periglacial Processes, 25:69-75.

Fu, P. and Rich, P. M. (1999). Design and implementation of the Solar Analyst: an ArcView extension for modeling solar radiation at landscape scales. 19th Annual ESRI User Conference, pages 1–24.

Garreaud, R. D. (2009). The Andes climate and weather. Advances in Geosciences, 22(22):3–11.

Gascoin, S., Kinnard, C., Ponce, R., Lhermitte, S., MacDonell, S., and Rabatel, A. (2011). Glacier contribution to streamflow in two headwaters of the Huasco River, Dry Andes of Chile. The Cryosphere, 5(4):1099–1113.

Giardino, J., Regmi, N., Vitek, J., (2014). Rock Glaciers. Encyclopedia of Snow, Ice and Glaciers. 943-948.

Gruber, S. and Hoelzle, M. (2001). Statistical modelling of mountain permafrost distribution: local calibration and incorporation of remotely sensed data. Permafrost and Periglacial Processes, 12(1):69–77.

Gruber, S. and Haeberli, W. (2009) Mountain Permafrost. Soil Biology PermafrostSoils. Vol 16: 33-66.

Haeberli, W., Hoelzle, M., Kääb, A., Keller, F., Muhil, D., Wagner, S. (1998). Ten years after drilling through the permafrost of the active rock glacier Murtel, Eastern Swiss Alps: Answered questions and new perspectives. Permafrost – Seventh International Conference (Proceedings), Collection Nordicana No. 55: 403-410.

Haeberli, W., Hallet, B., Arenson, L., Elconin, R., Humlum, O., Kääb, A., Kaufmann, V., Ladanyi, B., Matsuoka, N., Springman, S., Vonder Mühll, D. (2006). Permafrost creep and rock glacier dynamics. Permafrost and Periglacial Processes 17, 189–214.

Harris, C., Arenson, L., Christiansen, H., Etzelmuller, B., Frauenfelder, B., Gruber, S., Haeberli, W., Hauck, C., Hoelzle, M., Humlum, O., Isaksen, K., Kääb, A., Kern-Lütschg, M., Lehning, M., Matsuoka, N., Murton, J., Noetzli, J., Phillips, M., Ross, N., Seppälä, M., Springmanm, S., Vonder, MühllD. (2009). Permafrost and climate in Europe: monitoring and modelling thermal, geomorphological and geotechnical responses. Earth-Science Reviews 92, 117–171.

Heredia, N., Farias, P., García-Sansegundo, J., and Giambiagi, L. (2012). El Basamento de la Cordillera Frontal de los Andes en el Cordón del Plata (Mendoza, Argentina): Evolución Geodinámica. Andean geology, 39(2):242–257.

Huang, S. and Fu, P. (2009). Modeling small areas is a big challenge: using the solar radiation analysis tools in ArcGIS Spatial Analyst. ESRI ArcUser Online volume, pages 28–31.

Janke, J., Bellisario, A., Ferrando, F. (2015). Classification of debris-covered glaciers and rock glaciers in the Andes of central Chile. Geomorphology, 241: 98–121.

Lenzano, M., Leiva, J., Lenzano, L. (2010). Recent variation of the Las Vacas Glacier Mt. Aconcagua region, Central Andes, Argentina, based on ASTER stereoscopic images. Advances in Geosciences, 22: 185–189.

Lliboutry, L. (1998). Glaciers of Chile and Argentina. Geological Survey Professional Paper, 1386:1103.

Maksaev, V., Munizaga, F., Zentilli, M., Charrier, R. (2009). Fission track thermochronology of Neogene plutons in the Principal Andean Cordillera of central Chile (33-35°S): Implications for tectonic evolution and porphyry Cu-Mo mineralization. Andean Geology, 36(2): 153-171.

Martin, H. E., Whalley, W. B. (1987). Rock glaciers part 1, Rock glacier morphology: Classification and distribution. Progress in Physical Geography, 11(2): 260-282.

Maydagan, L., Franchini, M., Impiccini, A., Lentz, D. (2016). Phyllosilicates geochemistry and distribution in the Altar porphyry Cu-(Au) deposit, Andes Cordillera of San Juan, Argentina: Applications in exploration, geothermometry, and geometallurgy. Journal of Geochemical Exploration, 167: 83-109.

Millar, I., Westfall, R. (2008) Rock glaciers and related periglacial landforms in the Sierra Nevada, CA, USA; inventory, distribution and climatic relationships. Quaternary International, 188: 90–104.

Perucca, L., Angillieri, E. (2007). A preliminary inventory of periglacial landforms in the Andes of La Rioja and San Juan, Argentina, at about 28°S. Quaternary International, 190: 171-179.

Perucca, L., Angillieri, E. (2011). Glaciers and rock glaciers' distribution at 28°SL, Dry Andes of Argentina, and some considerations about their hydrological significance. Environmental Earth Science, 64: 2079-2089.

Rabassa, J. and Clapperton, C. M. (1990). Quaternary glaciations of the southern Andes. Quaternary Science Reviews, 9(2-3):153–174.

Ramos, V.A., Vujovich, G.I. (1995). Descripcio´n de la Hoja Geologica San Juan (1:250,000). Direccio´n Nacional del Servicio Geologico, Buenos Aires.

Rangecroft, S., Harrison, S., Anderson, K., Magrath, J., Castel, A., Pacheco P. (2014). A First Rock Glacier Inventory for the Bolivian Andes. Permafrost and Periglacial Processes 25 (4): 333-343.

Ruiz, L. and Trombotto Liaudat, D. (2012). Mountain permafrost distribution in the Andes of Chubut (Argentina) based on a statistical model. In Tenth International Conference on Permafrost.

Scotti, R., Brardinoni, F., Alberti, S., Frattini, P., Crosta, G. (2013). A regional inventory of rock glaciers and protalus ramparts in the central Italian Alps. Geomorphology, 186: 136–149.

Sloan, V., Dyke, L. (1998). Decadal and millennial velocities of rock glaciers, Selwyn Mountains, Canada. Geografiska Annaler. 80A (3–4): 237–249.

Schmid, M.-O., Baral, P., Gruber, S., Shahi, S., Shrestha, T., Stumm, D., and Wester, P. (2015). Assessment of permafrost distribution maps in the Hindu Kush Himalayan region using rock glaciers mapped in Google Earth. The Cryosphere, 9: 2089-2099.

Shakesby, R., Matthews, J., McEwen, L., Berrisford, M. (1999). Snow-push processes in pronival (protalus) rampart formation: geomorphological evidence from Smorbotn, Romsdalesalpane, southern Norway. Geografiska Annaler. 81A(1): 31-45.

Strecker, M., Alonso, R., Bookhagen, B., Carrapa, B., Hilley, G., Sobel, E., and Trauth, M. (2007). Tectonics and climate of the Southern Central Andes. Annual Review of Earth and Planetary Sciences, 35(1):747–787.

Trombotto, D., Buk, E., and Hernández, J. (1997). Monitoring of mountain permafrost in the central Andes, Cordon del Plata, Mendoza, Argentina. Permafrost and Periglacial Processes, 8(1):123–129.

Uyeda, S., Kanamori, H. (1979). Back-arc opening and the mode of subduction, Journal of Geophysics, 84(B3): 1049-1061.